NANO LETTERS

pubs.acs.org/NanoLett

Letter

Electrostatic Shielding Regulation of Magnetron Sputtered Al-Based Alloy Protective Coatings Enables Highly Reversible Zinc Anodes

Jiaxian Zheng, Zihao Huang, Ye Zeng, Wanqiang Liu,* Binbin Wei, Zhengbing Qi,* Zhoucheng Wang, Chuan Xia, and Hanfeng Liang*

Cite This: *Nano Lett.* 2022, 22, 1017−1023

Read Online

ACCESS | Metrics & More | Article Recommendations | Supporting Information

ABSTRACT: The uncontrolled zinc dendrite growth during plating leads to quick battery failure, which hinders the widespread applications of aqueous zinc-ion batteries. The growth of Zn dendrites is often promoted by the "tip effect". In this work, we propose a generate strategy to eliminate the "tip effect" by utilizing the electrostatic shielding effect, which is achieved by coating Zn anodes with magnetron sputtered Al-based alloy protective layers. The Al can form a surface insulating Al_2O_3 layer and by manipulating the Al content of Zn−Al alloy films, we are able to control the strength of the electrostatic shield, therefore realizing a long lifespan of Zn anodes up to 3000 h at a practical operating condition of 1.0 mA cm^{-2} and 1.0 mAh cm^{-2}. In addition, the concept can be extended to other Al-based systems such as Ti−Al alloy and achieve enhanced stability of Zn anodes, demonstrating the generality and efficacy of our strategy.

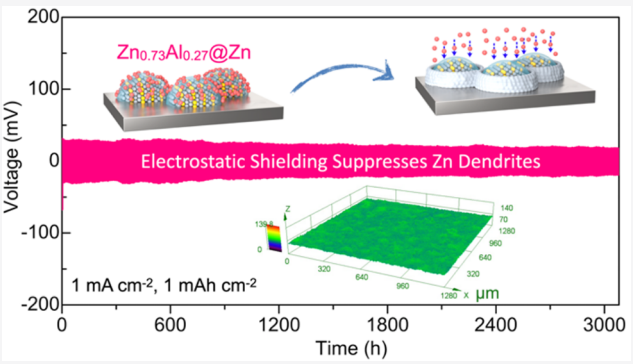

KEYWORDS: *Zn-ion batteries, metal anodes, electrostatic shielding, dendrite free, surface protective coatings*

Aqueous rechargeable zinc-ion batteries (ZIBs) are considered as a promising candidate for electric vehicles, mobile devices, and large-scale energy storage systems.[1−3] ZIBs utilize metallic Zn as an anode, which has many advantages including high volumetric/gravimetric capacity (5854 mAh cm^{-3} or 820 mAh g^{-1}), relatively low redox potential (−0.76 V vs. standard hydrogen electrode, or SHE), high safety, and low toxicity.[4−6] However, the utilization of Zn anode in ZIBs still faces many challenges, especially the Zn dendrite growth that would eventually lead to short-circuit and consequent battery failure, which hinders the widespread applications of ZIBs.[7] The "tip effect" caused by irregular and uncontrollable Zn deposition is the main reason for Zn dendrite growth.[8−10] During zinc plating process, Zn atoms tend to deposit onto specific sites with low energy barrier and grow into initial protuberances on Zn foil surface. The tips (protuberances) have a very high curvature and thus exhibit a higher local current density.[11] Zn^{2+} ions are then preferably adsorbed on these tips, which further accelerates the Zn dendrite growth.[12] Therefore, eliminating the "tip effect" is crucial to realizing the homogeneous distribution of current density and controllable Zn deposition.

Electrostatic shielding mechanism has been widely used as an effective way to eliminate the tip effect in lithium plating but has rarely been used to regulate the Zn deposition.[13−15] Electrolyte engineering is the main strategy to achieve the electrostatic shielding effect.[13,16−18] It often uses electrolyte additives that contain cations (M^+) with a lower reduction potential than the target metal ions (e.g., Zn^{2+}), which will not be electroplated but instead be adsorbed on the tips, thus forming an electrostatic shield.[18] The positively charged shield will repel the incoming charge carrier metal ions (i.e., Zn^{2+} in ZIBs) from the electrolyte because of the electrostatic repulsion, forcing them to be deposited onto adjacent regions of the tips.[13] In this way, the curvature of the tips will be decreased and therefore an evenly distributed local current density and the dendrite-free deposition can be achieved. However, the inevitable continuous depletion of electrolyte additives during cycling could lead to the weakening of electrostatic shielding effect and decrease the stability of the anodes. To avoid this issue, Jiang et al. designed a eutectic zinc−aluminum alloy that is composed of alternating zinc and aluminum nanolamellas as the anode for ZIBs.[19] The alloy anode showed enhanced lifespan. However, the fabrication of the alloy anode is complicated and unlikely to be scaled up, and it is difficult to delicately tune the electrostatic shielding strength. In addition, the stripping of Zn directly from alloy

Received: October 11, 2021
Revised: January 11, 2022
Published: January 18, 2022

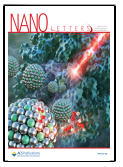

https://doi.org/10.1021/acs.nanolett.1c03917
Nano Lett. 2022, 22, 1017−1023

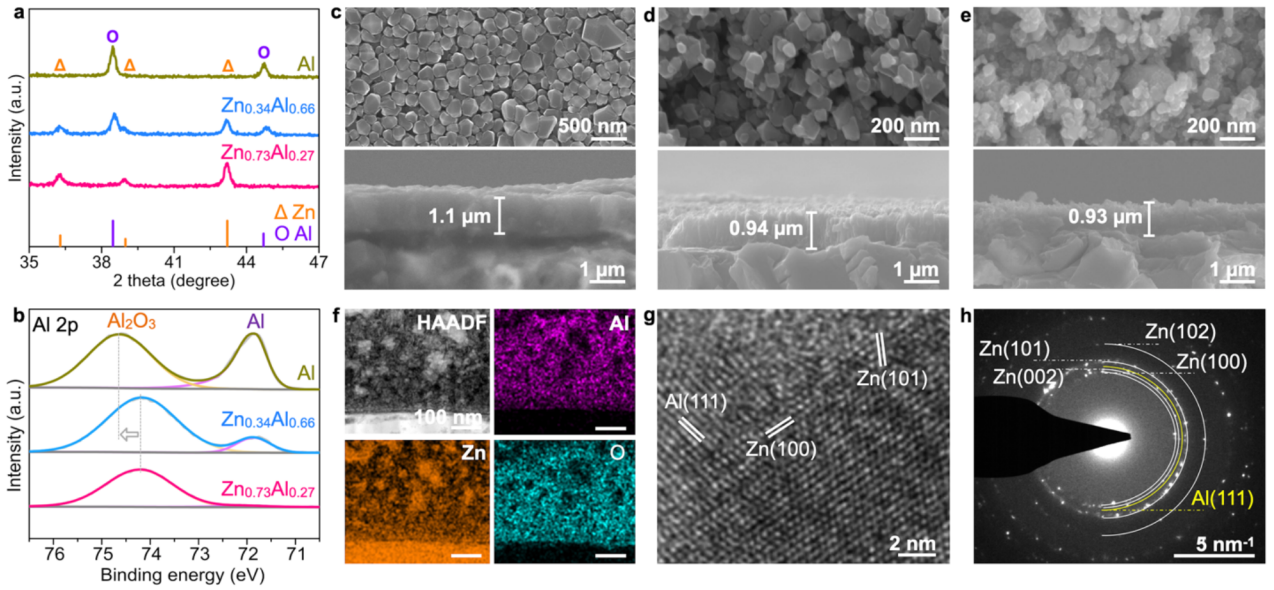

Figure 1. Structural characterization of Zn−Al alloy films. (a) XRD patterns and (b) Al 2p XPS spectra of Al, $Zn_{0.34}Al_{0.66}$, and $Zn_{0.73}Al_{0.27}$ films. SEM images of (c) Al, (d) $Zn_{0.34}Al_{0.66}$, and (e) $Zn_{0.73}Al_{0.27}$ coated Zn foils. (f) HADDF image and the corresponding elemental maps. (g) HRTEM image and (h) SAED pattern of the $Zn_{0.73}Al_{0.27}$ films.

might change the composition of the alloy and thus affect the electrostatic shielding effect. Therefore, it is desired to develop an alternative route to create the electrostatic shield with tunable strength.

Here, we proposed that Al-based alloys can function as effective protective layers for regulating the electrostatic shielding effect. Although Al possesses a lower redox potential of Al^{3+}/Al (−1.66 V vs SHE) than Zn^{2+}/Zn (−0.76 V vs SHE), it rapidly forms a stable insulating aluminum oxide (Al_2O_3) shell in aqueous solution, thus avoiding the dissolution of Al.[20] The Zn^{2+} ions will then be adsorbed on the Al_2O_3 shell and form an electrostatic shielding layer that prevents the further deposition of Zn^{2+} ions. In this work, we fabricated Al-based alloy films (i.e., Zn−Al and Ti−Al) using magnetron sputtering, a technique that is suitable for large-scale applications, which can not only precisely control the composition but also ensures good adhesion of the Zn anode and the alloy protective films without the use of binders. We found that the strength of electrostatic shield can be manipulated by adjusting the Al content in the alloy, therefore the tip effect can be effectively eliminated. In particular, the optimized Zn−Al alloy film-modified Zn anodes exhibit a long lifespan of over 3000 h at a practical current density/capacity of 1 mA/mAh cm^{-2}. Similar enhancement was also observed in the Ti−Al@Zn anode, further confirming the efficacy of regulating electrostatic shielding effect in enhancing Zn anode performance by engineering the Al-based alloy protective coatings.

Pure Al, $Zn_{0.34}Al_{0.66}$, and $Zn_{0.73}Al_{0.27}$ films were fabricated by magnetron sputtering (see Experimental Section in Supporting Information). The X-ray diffraction (XRD) peaks of the as-prepared samples are consistent with Al metal or Zn−Al alloys (JCDPS: Zn #65-5973 and Al #85-1327) (Figure 1a). The X-ray photoelectron spectroscopy (XPS) was then employed to probe the surface chemical states of Al and Zn elements. The peak at 72 eV in the Al 2p spectra can be assigned to metallic Al (Figure 1b), whereas the one at ∼74.3 eV is ascribed to the surface Al_2O_3 layer (Figure 1b).[19] The latter peak in pure Al layer shifts to higher binding energy, which is caused by the charge accumulation on the surface during the measurement. This phenomenon has been commonly observed in literature.[21] The existence of Al in $Zn_{0.73}Al_{0.27}$ is further confirmed by the XPS spectra of the etched samples (Figure S1). The Zn 2p and Zn LMM auger spectra suggest that the samples contain both the metallic Zn and Zn^{2+} species (Figures S2).[19] Scanning electron microscope (SEM) images show that all three films exhibit a porous structure consisted of numerous nanoparticles (Figures 1c−e). Energy dispersive spectroscopy (EDS) mapping further illustrates the even distribution of O, Al, and Zn elements (Figures S3). The three films possess similar thickness and roughness (Figure S4, and see the morphology of bare Zn in Figure S5). In general, a porous structure can increase the contact area between the anode surface and electrolyte. Indeed, the water contact angles of the Zn−Al alloys are smaller than those of the bare Zn and pure Al films (Figure S6), indicating the improved surface wettability. In order to further investigate the microstructure of the $Zn_{0.73}Al_{0.27}$ films, we conducted HADDF (high-angle annular dark-field) imaging (Figure 1f). The HAADF image and the corresponding element maps further confirm the existence of O, Al and Zn in $Zn_{0.73}Al_{0.27}$ films. The high-resolution transmission electron microscopy (HRTEM) image (Figure 1g) and the selected area electron diffraction (SAED) pattern (Figure 1h) illustrate the coexistence of metallic Zn and Al, which is consistent with the XRD result.

To evaluate the electrochemical performance of Zn−Al alloy protected Zn anodes, symmetric batteries were assembled and tested under a constant current density/capacity of 1.0 mA/mAh cm^{-2}. As shown in Figure 2a, the Al@Zn and $Zn_{0.34}Al_{0.66}$@Zn anodes suffer from rapid short-circuit after 130 h, which are even inferior to the bare Zn anode (180 h). This result indicates that Al-rich protective alloy layers cannot inhibit the Zn dendrite growth. In sharp contrast, the $Zn_{0.73}Al_{0.27}$@Zn anodes deliver an outstanding cycling stability for at least 3000 h. In addition, it shows a lower voltage hysteresis (48.3 mV) than that of the bare Zn (63.8 mV), Al@

https://doi.org/10.1021/acs.nanolett.1c03917
Nano Lett. 2022, 22, 1017−1023

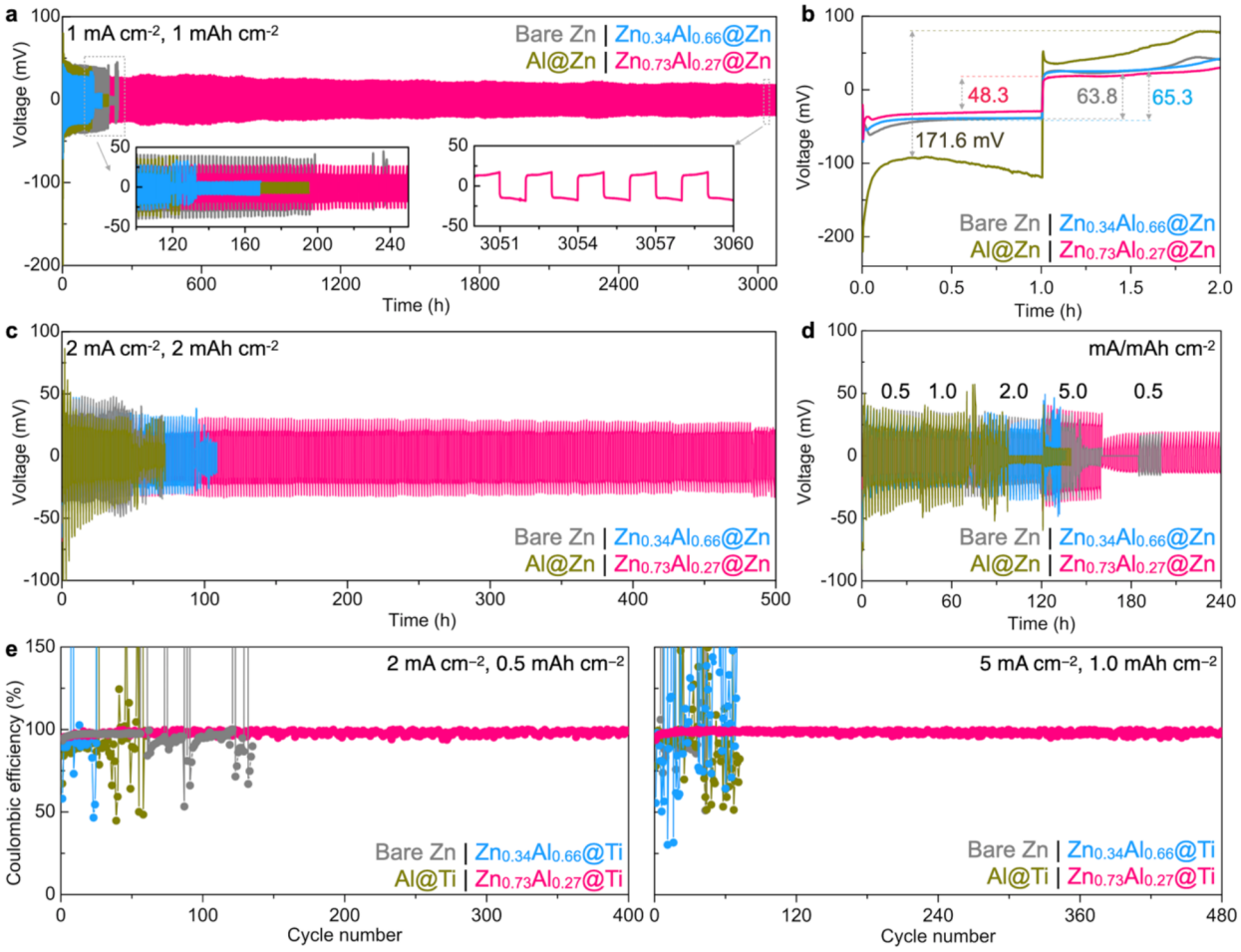

Figure 2. Electrochemical performance of Zn−Al coated Zn anodes. (a) Galvanostatic cycling of symmetric cells at 1 mA cm^2 and 1 mAh cm^{-2}, and (b) the corresponding voltage hysteresis of the first cycle. (c) Galvanostatic cycling of symmetric cells at 2 mA cm^2 and 2 mAh cm^{-2}. (d) Rate performance at current densities from 0.5 to 5 mA cm^{-2} with a constant charge and discharge time of 1 h. (e) Coulombic efficiencies of the various Zn electrodes at different conditions.

Zn (171.6 mV), and $Zn_{0.34}Al_{0.66}$@Zn (65.3 mV) at the first cycle (Figure 2b), suggesting that a proper Al content can significantly enhance the lifespan. The small polarization represents a low energy barrier for Zn nucleation.[22] The trend in nucleation overpotential of the four samples can be further verified by the voltage profiles as shown in Figure S7. There are significant voltage drops at the beginning of the Zn metal deposition, followed by a flat voltage plateau. The overpotential represents the heterogeneous nucleation barrier that needs to be overcome for Zn deposition which is defined as the difference between the bottom of the voltage dip and the flat voltage plateau.[23] For bare stainless steel (SS) substrate, the overpotential is about 50 mV. As for Al@SS, a higher overpotential (~72 mV) is required. This is because the Al is covered by the insulating Al_2O_3 surface layer, which would produce a strong electrostatic shield and thus increase the Zn nucleation barrier. In contrast, the $Zn_{0.34}Al_{0.66}$@SS and $Zn_{0.73}Al_{0.27}$@SS possess lower overpotentials of 24 and 22 mV, respectively, which indicate the presence of metallic Zn in the alloys favors the nucleation and growth of Zn. It is noted that the cycling stability sensitively relies on the ratio of Al/Zn in the alloy protective layers. The $Zn_{0.73}Al_{0.27}$@Zn possesses a much longer lifespan than $Zn_{0.34}Al_{0.66}$@Zn. This is because that a high Al/Zn ratio would create a strong electrostatic shield, forcing Zn^{2+} ions to be deposited onto the limited metallic Zn sites, which therefore accelerates the growth of Zn dendrites. On the other hand, a relatively low Al/Zn ratio could produce an electrostatic shield with moderate strength, while there are still sufficient Zn sites for Zn plating, which essentially leads to an even Zn deposition. Figure 2c compares the performance of various Zn anodes under high current density, and the $Zn_{0.73}Al_{0.27}$@Zn exhibits the best performance that can stably cycle for at least 500 h at 2.0 mA/mAh cm^{-2}. However, the other three cells suffer from quick battery failure during the cycling at the same testing conditions. Moreover, the $Zn_{0.73}Al_{0.27}$@Zn electrodes also exhibit stable and flat plateaus at various current densities (Figure 2d). The voltage hysteresis is as small as ~72 mV even at a high rate of 5 mA cm^{-2}, and quickly drops to ~44 mV that is close to the initial value in response to the current recovering to 0.5 mA cm^{-2}. We further evaluated the Coulombic efficiency using a reported protocol.[24] The result reveals that the Zn||$Zn_{0.73}Al_{0.27}$@Ti cell possesses steady Coulombic efficiencies (CEs) of 99.25% and 99.13% at 2 and 5 mA cm^{-2}, respectively, as well as high stability for more than 400 h (Figure 2e). In contrast, the other three cells suffer from instable CE and low lifespan. These results confirm that the Zn−Al alloy films with

https://doi.org/10.1021/acs.nanolett.1c03917
Nano Lett. 2022, 22, 1017−1023

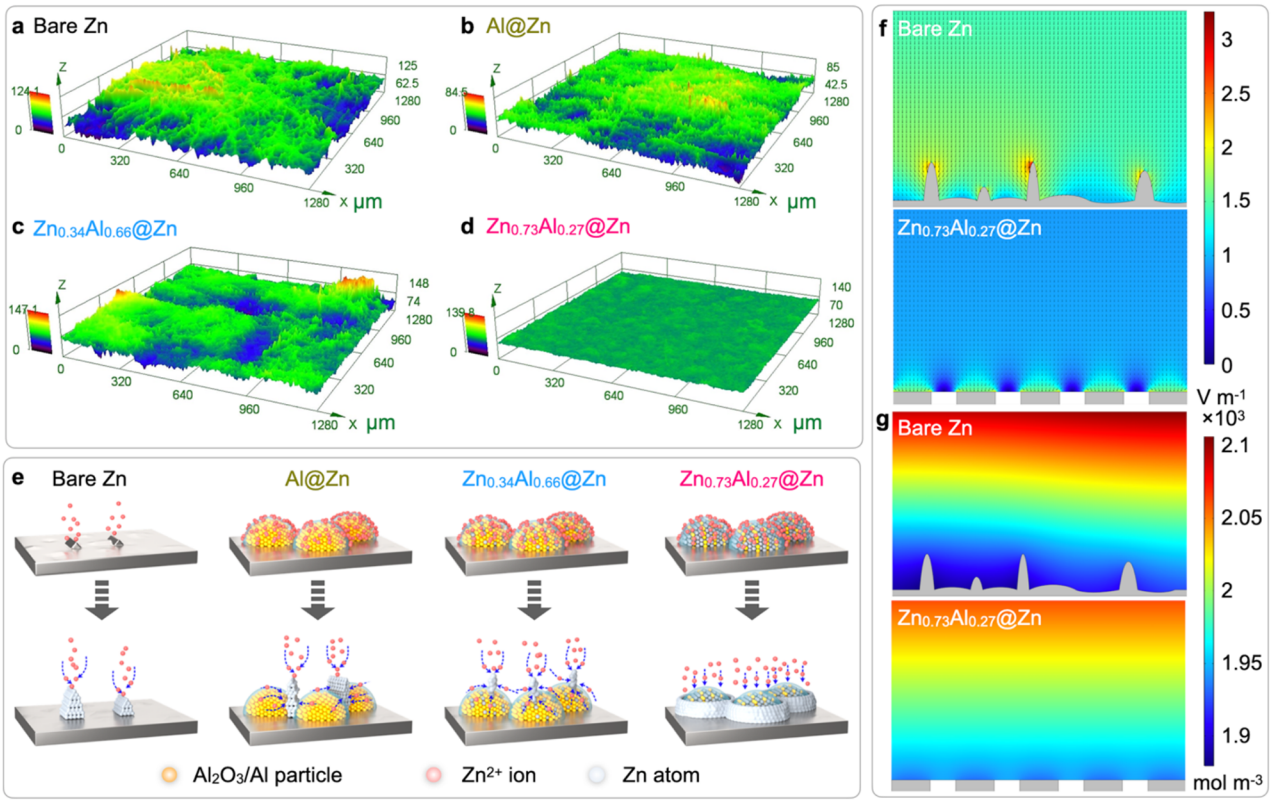

Figure 3. Structural evolution of various Zn electrodes. The 3D CLSM images of (a) bare Zn, (b) Al@Zn, (c) $Zn_{0.34}Al_{0.66}$@Zn, and (d) $Zn_{0.73}Al_{0.27}$@Zn after 24 h cycling. (e) Schematic illustration of Zn deposition on different Zn electrodes. Simulated (f) electric field and (g) Zn^{2+} ion distribution of the bare Zn and $Zn_{0.73}Al_{0.27}$@Zn surfaces.

a proper Al content can effectively enhance the Zn anode performance.

In order to further investigate the impact of the Zn−Al alloy films on the structural evolution of the Zn anodes, we conducted confocal laser scanning microscopy (3D CLSM) characterization of the bare Zn, Al@Zn, $Zn_{0.34}Al_{0.66}$@Zn, and $Zn_{0.73}Al_{0.27}$@Zn symmetric cells after cycling for 24 h at 1.0 mA/mAh cm^{-2}. The result reveals that the surface (with a large area of 1280 μm × 1280 μm) of $Zn_{0.73}Al_{0.27}$@Zn anode after cycling is still flat, whereas the other three show a much rougher surface where the Zn dendrites can be clearly seen (Figure 3a−d). In addition, the SEM observation also suggests the same phenomenon (Figure S8), further confirming that the optimized electrostatic field of $Zn_{0.73}Al_{0.27}$ can effectively suppress the Zn dendritic growth. It should be noted that there was no detectable Al^{3+} ions in the electrolyte after 1 h cycling by the inductively coupled plasma optical emission spectroscopy (ICP-OES), indicating the high chemical stability of Al in Zn−Al alloys. The electrochemical impedance spectroscopy (EIS) result shows that the charge transfer resistance of the $Zn_{0.73}Al_{0.27}$@Zn is lower than that of the bare Zn, Al@Zn, and $Zn_{0.34}Al_{0.66}$@Zn, suggesting a more efficient charge transfer process (Figure S9).[19,25] The XRD pattern of $Zn_{0.73}Al_{0.27}$@Zn after cycling for 24 h at a higher current density/areal capacity (2.0 mA/mAh cm^{-2}) reveals a much low peak intensity of the byproduct ($Zn_4SO_4(OH)_6{\cdot}H_2O$, or ZHS) than that of bare Zn, suggesting that the Zn−Al coatings also effectively suppress the side reactions (Figure S10). After long-term cycling, big Zn dendrites/tips are observed on the bare Zn, Al@Zn, and $Zn_{0.34}Al_{0.66}$@Zn electrodes, which directly cause short-circuits (Figure S8e−g). However, the $Zn_{0.73}Al_{0.27}$@Zn remains a relatively smooth surface even after cycling for a much longer time of 1800 h, confirming the outstanding cycling performance of the $Zn_{0.73}Al_{0.27}$@Zn electrodes (Figure S8h and Figure S11). Indeed, the thickness of $Zn_{0.73}Al_{0.27}$ alloy film barely changes after 24 h cycling and is only increased by 35% after 1800 h (Figure S12). This result further confirms the high chemical and mechanical stability of the $Zn_{0.73}Al_{0.27}$ alloy films.

According to the above results, the diffusion and deposition behavior of Zn^{2+} ions can be manipulated by tuning the Al content of the alloy protective coatings. The Zn deposition on the surfaces of the bare Zn, Al@Zn, $Zn_{0.34}Al_{0.66}$@Zn, and $Zn_{0.73}Al_{0.27}$@Zn anodes are schematically illustrated in Figure 3e. On the bare Zn anode surface, Zn^{2+} ions tend to deposit on the tips with a low nucleation barrier, leading to the growth of Zn dendrites upon continuous cycling. As for the Al@Zn, the Al is coated by an *in situ* formed dense insulating Al_2O_3 layer. As a result, the Zn^{2+} ions can only diffuse through the porous Al films (Figure 1c) and then deposit onto the underneath Zn foil. The subsequent Zn ions will preferentially deposit on the previously formed zinc nuclei to lower the nucleation energy, which would eventually result in the growth of Zn dendrites. Similarly, the protective coatings with a high Al (i.e., $Zn_{0.34}Al_{0.66}$@Zn) content also suffer from the above obstacles. Zn^{2+} ions will preferentially deposit on the limited Zn sites, which promotes the growth of Zn dendrites. In contrast, a proper Al content (i.e., $Zn_{0.73}Al_{0.27}$@Zn) would produce a moderate strength of electrostatic shield, thus forcing the Zn ions to be evenly deposited onto the separately distributed Zn sites, which avoids the excessive accumulation of Zn deposits and thus dendrites. This eventually leads to a significantly

https://doi.org/10.1021/acs.nanolett.1c03917
Nano Lett. 2022, 22, 1017−1023

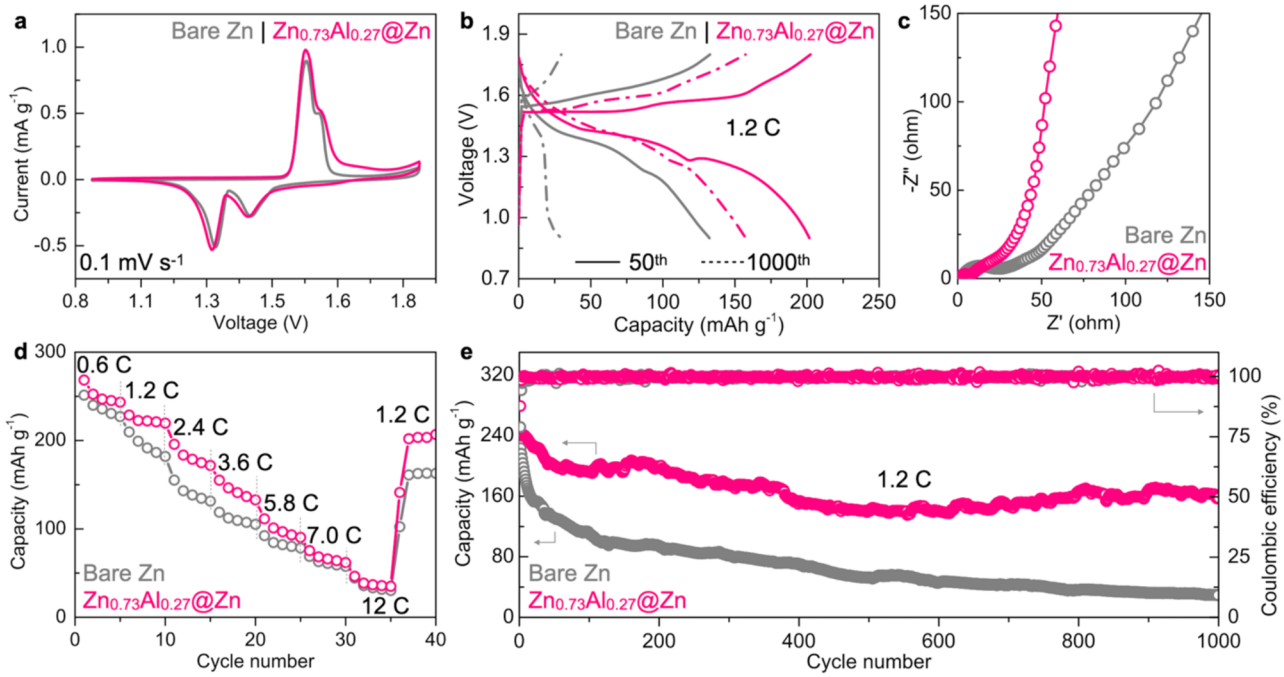

Figure 4. Electrochemical performance of $Zn_{0.73}Al_{0.27}$@Zn||MnO_2 full cells. (a) CV curves of the first cycle at 0.1 mV s^{-1}, (b) charge/discharge curves at 1.2 C, (c) EIS spectra before cycling, (d) rate performance, and (e) cycling stability at 1.2 C of the $Zn_{0.73}Al_{0.27}$@Zn||MnO_2 and Zn||MnO_2 full cells.

improved lifespan of Zn anodes. To further illustrate the role of $Zn_{0.73}Al_{0.27}$ alloy film in regulating the electric field and Zn^{2+} ion distribution at the anode surface, a theoretical simulation was carried out using COMSOL (Figure 3f,g). The electric field and Zn^{2+} ion distribution on the bare Zn surface display an obvious intensity gradient during the Zn plating process. Such enhanced local electric field and uneven ionic distribution create a charge accumulated region, thus promoting Zn^{2+} deposition onto the specific sites. Because of the "tip effect", these small protuberances gradually evolve into large Zn dendrites. In contrast, the uniformly distributed electric field and Zn^{2+} ions ensure homogeneous Zn^{2+} deposition on the surface, thereby maintaining a flat and smooth surface even after long cycling. This theoretical result further explains the enhanced performance of the $Zn_{0.73}Al_{0.27}$@Zn electrodes.

The above results have shown the overall performance of Zn anodes can be improved by regulating the electrostatic shielding strength of the surface protective coatings. The versatility of our strategy was further verified by the enhanced stability of Ti−Al alloy protected Zn anodes (see characterization and electrochemical performance of Ti−Al@Zn in Figures S13−S16), To further evaluate the particle application, the performance of the $Zn_{0.73}Al_{0.27}$@Zn||MnO_2 full cells (see the characterization of MnO_2 cathodes in Figure S17) were tested and compared with unmodified Zn||MnO_2 cells. The electrolyte was a solution of 2 M $ZnSO_4$ and 0.1 M $MnSO_4$. Cyclic voltammetry (CV) curves show almost the same shape and two pairs of redox peaks that are associated with the oxidation/reduction of Mn(IV) to Mn(III)/Mn(II) species (Figure 4a). Whereas the $Zn_{0.73}Al_{0.27}$@Zn||MnO_2 batteries exhibit a bigger integrated area than that of the bare Zn||MnO_2 batteries during the first cycle, indicating the enhanced capacity. The charge−discharge profiles of the $Zn_{0.73}Al_{0.27}$@Zn||MnO_2 batteries show a more stable voltage plateau and a narrower voltage gap than that of the bare Zn||MnO_2 after 50 and 1000 cycles (Figure 4b). The EIS result suggests that batteries with $Zn_{0.73}Al_{0.27}$ alloy films possess a lower charge transfer resistance and a faster Zn^{2+} ions diffusion kinetics than that of with bare Zn electrodes (Figure 4c). This result is consistent with the symmetric cell measurements. The rate performance of the $Zn_{0.73}Al_{0.27}$@Zn||MnO_2 and bare Zn||MnO_2 batteries at various current densities from 0.6 to 12 C (1 C = 616 mA g^{-1}) is displayed in Figure 4d. The capacity of $Zn_{0.73}Al_{0.27}$@Zn||MnO_2 battery returns to about 203 mAh g^{-1} (at 1.2 C) after cycling at a high current density (12 C), which is higher than that of bare Zn||MnO_2 cell (162 mAh g^{-1}). More importantly, the capacity of $Zn_{0.73}Al_{0.27}$@Zn||MnO_2 battery remains about 163 mAh g^{-1} (67% retention) after 1000 cycles, which is dramatically higher than that of the bare Zn||MnO_2 (30 mAh g^{-1}, 13% retention) (Figure 4e). These results confirm that the $Zn_{0.73}Al_{0.27}$ alloy films can significantly boost the performance of Zn anodes in terms of both the capacity and stability.

CONCLUSION

In summary, we proposed a generate strategy to significantly enhance the cycling stability of Zn anodes by electrostatic shielding manipulation. Specially, we prepared Zn−Al alloys using magnetron sputtering and further investigated the impact of Al content on the electrochemical performance of Zn anodes. We found that a proper Al content leads to the optimized strength of electrostatic shielding, therefore resulting in a greatly prolonged cycling lifespan of at least 3000 h at 1 mA cm^{-2} and 1 mAh cm^{-2}. The versatility of this strategy was further verified by the Ti−Al alloy protective layers. Our work highlights the important role of Al sites in regulating the electrostatic shielding effect to achieve stable Zn plating and further provides insights into the design of surface protective layers for high performance ZIBs and potentially other multivalent ion batteries.

https://doi.org/10.1021/acs.nanolett.1c03917
Nano Lett. 2022, 22, 1017−1023

■ ASSOCIATED CONTENT

Supporting Information

The Supporting Information is available free of charge at https://pubs.acs.org/doi/10.1021/acs.nanolett.1c03917.

Additional XRD patterns, SEM and AFM images and electrochemical data (PDF)

■ AUTHOR INFORMATION

Corresponding Authors

Wanqiang Liu − *School of Materials Science and Engineering, Changchun University of Science and Technology, Changchun 130022, China;* orcid.org/0000-0003-1606-9232; Email: wqliu1979@126.com

Zhengbing Qi − *Key Laboratory of Functional Materials and Applications of Fujian Province, School of Materials Science and Engineering, Xiamen University of Technology, Xiamen 361024, China*; Email: zbqi@xmut.edu.cn

Hanfeng Liang − *State Key Laboratory of Physical Chemistry of Solid Surfaces, College of Chemistry and Chemical Engineering, Xiamen University, Xiamen 361005, China;* orcid.org/0000-0002-1778-3975; Email: hfliang@xmu.edu.cn

Authors

Jiaxian Zheng − *State Key Laboratory of Physical Chemistry of Solid Surfaces, College of Chemistry and Chemical Engineering, Xiamen University, Xiamen 361005, China*

Zihao Huang − *State Key Laboratory of Physical Chemistry of Solid Surfaces, College of Chemistry and Chemical Engineering, Xiamen University, Xiamen 361005, China*

Ye Zeng − *State Key Laboratory of Physical Chemistry of Solid Surfaces, College of Chemistry and Chemical Engineering, Xiamen University, Xiamen 361005, China*

Binbin Wei − *Shenzhen Geim Graphene Center, Tsinghua-Berkeley Shenzhen Institute and Tsinghua Shenzhen International Graduate School, Tsinghua University, Shenzhen 518055, China*

Zhoucheng Wang − *State Key Laboratory of Physical Chemistry of Solid Surfaces, College of Chemistry and Chemical Engineering, Xiamen University, Xiamen 361005, China*

Chuan Xia − *Yangtze Delta Region Institute (Huzhou), University of Electronic Science and Technology of China, Huzhou 313001 Zhejiang, China; School of Materials and Energy, University of Electronic Science and Technology of China, Chengdu 611731, China;* orcid.org/0000-0003-4526-159X

Complete contact information is available at: https://pubs.acs.org/10.1021/acs.nanolett.1c03917

Author Contributions

The manuscript was written through contributions of all authors. All authors have given approval to the final version of the manuscript

Notes

The authors declare no competing financial interest.

■ ACKNOWLEDGMENTS

This work was supported by the National Natural Science Foundation of China (Grants 22001081, 22075236, 51601163), National Key R&D Program of China (2017YFE0198100), Natural Science Foundation of Fujian Province (2021J011211), and Xiamen University.

■ REFERENCES

(1) Zhang, L.; Hou, Y. Comprehensive Analyses of Aqueous Zn Metal Batteries: Characterization Methods, Simulations, and Theoretical Calculations. *Adv. Energy Mater.* **2021**, *11*, 2003823.

(2) Blanc, L.; Kundu, D.; Nazar, L. Scientific Challenges for the Implementation of Zn-Ion Batteries. *Joule* **2020**, *4*, 771−799.

(3) Hu, L.; Xiao, P.; Xue, L.; Li, H.; Zhai, T. The Rising Zinc Anodes for High-Energy Aqueous Batteries. *EnergyChem.* **2021**, *3*, 100052.

(4) Yi, Z.; Chen, G.; Hou, F.; Wang, L.; Liang, J. Strategies for the Stabilization of Zn Metal Anodes for Zn-Ion Batteries. *Adv. Energy Mater.* **2021**, *11*, 2003065.

(5) Pan, Z.; Liu, X.; Yang, J.; Li, X.; Liu, Z.; Loh, X.; Wang, J. Aqueous Rechargeable Multivalent Metal-Ion Batteries: Advances and Challenges. *Adv. Energy Mater.* **2021**, *11*, 2100608.

(6) Liu, Z.; Huang, Y.; Huang, Y.; Yang, Q.; Li, X.; Huang, Z.; Zhi, C. Voltage Issue of Aqueous Rechargeable Metal-Ion Batteries. *Chem. Soc. Rev.* **2020**, *49*, 180−232.

(7) Tang, B.; Shan, L.; Liang, S.; Zhou, J. Issues and Opportunities Facing Aqueous Zinc-Ion Batteries. *Energy Environ. Sci.* **2019**, *12*, 3288−3304.

(8) Yang, Q.; Li, Q.; Liu, Z.; Wang, D.; Guo, Y.; Li, X.; Tang, Y.; Li, H.; Dong, B.; Zhi, C. Dendrites in Zn-Based Batteries. *Adv. Mater.* **2020**, *32*, 2001854.

(9) Zhang, Q.; Luan, J.; Tang, Y.; Ji, X.; Wang, H. Interfacial Design of Dendrite-Free Zinc Anodes for Aqueous Zinc-Ion Batteries. *Angew. Chem., Int. Ed.* **2020**, *59*, 13180−13191.

(10) Verma, V.; Kumar, S.; Manalastas, W.; Srinivasan, M. Undesired Reactions in Aqueous Rechargeable Zinc Ion Batteries. *ACS Energy Lett.* **2021**, *6*, 1773−1785.

(11) Cui, B.; Han, X.; Hu, W. Micronanostructured Design of Dendrite-Free Zinc Anodes and Their Applications in Aqueous Zinc-Based Rechargeable Batteries. *Small Struct.* **2021**, *2*, 2000128.

(12) Lu, W.; Zhang, C.; Zhang, H.; Li, X. Anode for Zinc-Based Batteries: Challenges, Strategies, and Prospects. *ACS Energy Lett.* **2021**, *6*, 2765−2785.

(13) Ding, F.; Xu, W.; Graff, G.; Zhang, J.; Sushko, M.; Chen, X.; Shao, Y.; Engelhard, M.; Nie, Z.; Xiao, J.; Liu, X.; Sushko, P.; Liu, J.; Zhang, J. Dendrite-Free Lithium Deposition via Self-Healing Electrostatic Shield Mechanism. *J. Am. Chem. Soc.* **2013**, *135*, 4450−6.

(14) Ma, J.; Meng, F.; Yu, Y.; Liu, D.; Yan, J.; Zhang, Y.; Zhang, X.; Jiang, Q. Prevention of Dendrite Growth and Volume Expansion to Give High-Performance Aprotic Bimetallic Li-Na Alloy-O_2 Batteries. *Nat. Chem.* **2019**, *11*, 64−70.

(15) Xu, W.; Zhao, K.; Huo, W.; Wang, Y.; Yao, G.; Gu, X.; Cheng, H.; Mai, L.; Hu, C.; Wang, X. Diethyl Ether as Self-Healing Electrolyte Additive Enabled Long-Life Rechargeable Aqueous Zinc Ion Batteries. *Nano Energy* **2019**, *62*, 275−281.

(16) Li, Y.; Wu, P.; Zhong, W.; Xie, C.; Xie, Y.; Zhang, Q.; Sun, D.; Tang, Y.; Wang, H. A Progressive Nucleation Mechanism Enables Stable Zinc Stripping-Plating Behavior. *Energy Environ. Sci.* **2021**, *14*, 5563−5571.

(17) Wang, P.; Xie, X.; Xing, Z.; Chen, X.; Fang, G.; Lu, B.; Zhou, J.; Liang, S.; Fan, H. Mechanistic Insights of Mg^{2+}-Electrolyte Additive for High-Energy and Long-Life Zinc-Ion Hybrid Capacitors. *Adv. Energy Mater.* **2021**, *11*, 2101158.

(18) Wan, F.; Zhang, L.; Dai, X.; Wang, X.; Niu, Z.; Chen, J. Aqueous Rechargeable Zinc/Sodium Vanadate Batteries with Enhanced Performance from Simultaneous Insertion of Dual Carriers. *Nat. Commun.* **2018**, *9*, 1656.

(19) Wang, S.; Ran, Q.; Yao, R.; Shi, H.; Wen, Z.; Zhao, M.; Lang, X.; Jiang, Q. Lamella-Nanostructured Eutectic Zinc-Aluminum Alloys as Reversible and Dendrite-Free Anodes for Aqueous Rechargeable Batteries. *Nat. Commun.* **2020**, *11*, 1634.

(20) Faegh, E.; Ng, B.; Hayman, D.; Mustain, W. E. Practical Assessment of the Performance of Aluminium Battery Technologies. *Nat. Energy* **2021**, *6*, 21−29.
(21) Rosenberger, L.; Baird, R.; McCullen, E.; Auner, G.; Shreve, G. Xps Analysis of Aluminum Nitride Films Deposited by Plasma Sourcemolecular Beam Epitaxy. *Surf. Interface Anal.* **2008**, *40*, 1254−1261.
(22) Kang, L.; Cui, M.; Jiang, F.; Gao, Y.; Luo, H.; Liu, J.; Liang, W.; Zhi, C. Nanoporous $CaCO_3$ Coatings Enabled Uniform Zn Stripping/Plating for Long-Life Zinc Rechargeable Aqueous Batteries. *Adv. Energy Mater.* **2018**, *8*, 1801090.
(23) Yan, K.; Lu, Z.; Lee, H.; Xiong, F.; Hsu, P. C.; Li, Y.; Zhao, J.; Chu, S.; Cui, Y. Selective Deposition and Stable Encapsulation of Lithium through Heterogeneous Seeded Growth. *Nat. Energy* **2016**, *1*, 1−8.
(24) Ma, L.; Schroeder, M. A.; Borodin, O.; Pollard, T. P.; Ding, M. S.; Wang, C.; Xu, K. Realizing High Zinc Reversibility in Rechargeable Batteries. *Nat. Energy* **2020**, *5*, 743−749.
(25) Li, S.; Fu, J.; Miao, G.; Wang, S.; Zhao, W.; Wu, Z.; Zhang, Y.; Yang, X. Toward Planar and Dendrite-Free Zn Electrodepositions by Regulating Sn-Crystal Textured Surface. *Adv. Mater.* **2021**, *33*, 2008424.

https://doi.org/10.1021/acs.nanolett.1c03917
Nano Lett. 2022, 22, 1017−1023